Published in final edited form as:
J Neurosci. 2010 July 28; 30(30): 10076–10085. doi:10.1523/JNEUROSCI.6309-09.2010.

Coalescence and Fragmentation of Cortical Networks During Focal Seizures

Mark A. Kramer[1], **Uri T. Eden**[1], **Eric D. Kolaczyk**[1], **Rodrigo Zepeda**[2], **Emad N. Eskandar**[3,4], and **Sydney S. Cash**[2,4]

[1]Department of Mathematics and Statistics, Boston University, Boston, MA, 02215

[2]Department of Neurology, Massachusetts General Hospital, Boston, MA, 02114

[3]Department of Neurosurgery, Massachusetts General Hospital, Boston, MA, 02114

[4]Harvard Medical School, Boston, MA, 02115

Abstract

Epileptic seizures reflect a pathological brain state characterized by specific clinical and electrical manifestations. The proposed mechanisms are heterogeneous but united by the supposition that epileptic activity is hypersynchronous across multiple scales. Yet, principled and quantitative analyses of seizure dynamics across space and throughout the entire ictal period are rare. To more completely explore spatiotemporal interactions during seizures, we examined electrocorticogram (ECoG) data from a population of male and female human patients with epilepsy and from these data constructed dynamic network representations using statistically robust measures. We found that these networks evolved through a distinct topological progression during the seizure. Surprisingly, the overall synchronization changed only weakly while the topology changed dramatically in organization. A large subnetwork dominated the network architecture at seizure onset and preceding termination, but in between fractured into smaller groups. Common network characteristics appeared consistently for a population of subjects and, for each subject, similar networks appeared from seizure to seizure. These results suggest that, at the macroscopic spatial scale, epilepsy is not so much a manifestation of hypersynchrony but instead of network reorganization.

Keywords

Intracranial EEG; networks; dynamic connectivity; epilepsy; synchronization

INTRODUCTION

Epilepsy is a devastating disease affecting some 50 million people worldwide. Although manifesting as specific clinical symptoms, epilepsy is perhaps best characterized as a disease of brain rhythms — a paroxysmal cerebral dysrhythmia (Gibbs et al., 1937). Understanding how this dysrhythmia propagates and is maintained is a key problem in the treatment of epilepsy. From a simplistic perspective, focal seizures can be understood as local events beginning in a circumscribed region with the potential to recruit connected areas in a cascade of spreading activity from the central focus outwards through both pathological and normal brain tissue.

Address for correspondence: Mark A. Kramer, Boston University, Department of Mathematics and Statistics, 111 Cummington St, Boston MA, 02215, mak@bu.edu, Telephone: 1-617-353-4591.

Presumably, changes in synchronization between brain regions underlie the mechanisms of seizure spread. Classically, seizures are thought to represent a hypersynchronous state (Penfield and Jasper, 1954). To be detected as voltage fluctuations at the scalp surface there must be a sufficient number of simultaneously active neurons and synapses, so at some spatial scale increased synchrony must occur. Yet, recent observations challenge the formal assertion of hypersynchrony at larger spatial scales (Jerger et al., 2005; Schindler et al., 2007), in *in vitro* recordings of experimental seizures (Netoff and Schiff, 2002), and in human temporal lobe seizures (Bartolomei et al., 1999; Bartolomei et al., 2004; Guye et al., 2006; Ponten et al., 2007).

To understand seizure spread, synchronization measures are applied to the brain's voltage activity (Brazier, 1973; Gotman, 1983; Towle et al., 1999; Bartolomei et al., 1999; Wendling et al., 2003; Ferri et al., 2004; Bartolomei et al., 2004; Guye et al., 2006). For a few electrode pairs, these synchronization metrics are easily constructed and readily interpreted. However, for high-density electrode grids, complex functional topologies result whose quantitative understanding requires graph theory and network analysis techniques (Bullmore and Sporns, 2009; Reijneveld et al., 2007). Using these tools, specific network structures are revealed during the seizure, including such architecture patterns as small-world networks (Netoff et al., 2004; Ponten et al., 2007) and hubs (Morgan and Soltesz, 2008; Kramer et al., 2008).

In this paper, we analyze the dynamics of functional networks through the entire seizure in intracranial electrocorticogram (ECoG) recordings from a population of patients with intractable focal epilepsy. We show that some network properties are preserved while others change dramatically and predictably during initiation, propagation, and termination of the seizure. Analysis of the evolving networks suggests that, no matter what the cause of the particular focal epilepsy, stereotyped network patterns emerge. We propose that the changing synchronization structure of the seizure activity provides new insights into the mechanisms of seizures and novel intervention strategies. The analysis also suggests that seizures represent a paroxysmal cerebral dysrhythmia whose synchronization evolves through characteristic functional topologies without necessarily representing large scale hypersynchrony.

MATERIALS AND METHODS

Patients

Electrocorticography from 48 seizures (from 2 to 8 seizures [mean 4.4] per patient) in 11 patients (6 women, mean age at surgery of 37.4 years with a minimum age of 19 and maximum of 65) with long-standing pharmaco-resistant complex partial seizures (mean age at onset 20.2 years and mean duration of epilepsy of 17.3 years) were analyzed (Table 1). Patients were selected who were known to have seizures with focal onset and typical complex partial events often with secondary generalization. All recordings were performed using a standard clinical recording system (Xltek (subsidiary of Natus Medical Inc,) Oakville, Canada) with a 500 Hz sampling rate. Analysis of the data from these patients was performed retrospectively under protocols monitored by the local Institutional Review Boards according to NIH guidelines. Two-dimensional subdural electrode arrays as well as linear arrays of electrodes penetrating the brain (grid/strips and depth electrodes respectively, Ad-tech Medical, Racine, WI) were placed in order to confirm the hypothesized seizure focus, and locate epileptogenic tissue in relation to essential cortex, thus directing surgical treatment. Of the 11 patients, 5 were investigated with a combination of surface electrodes placed on the pia (grids and strips) as well as depth electrodes placed through the cortex to sample mesial structures (e.g. hippocampus, amygdala, cingulated gyrus, etc). Six patients had just depth electrodes placed. All patients had some sampling of

both neocortical structures and the mesial temporal lobe. As a result, all of the recordings possessed three-dimensional coverage of brain structures. Although extensive, these recordings do not permit observation of the entire brain; unobserved structures may play a role in the seizure process. The reference electrode was an electrode either placed on the neck (at the spinous process of the 2nd cervical vertebrate) or a strip of electrodes placed outside the dura and facing the skull at a region remote from the other grid and strip electrodes. The decision to implant, the electrode targets and the duration of implantation were made entirely on clinical grounds without reference to this research study.

Multiple etiologies were represented including mesial temporal sclerosis as diagnosed by history, seizure semiology and imaging (n=3); cortical dysplastic lesions confirmed with pathology (n=2); post-traumatic epilepsy (n=1) and sequelae from a presumed viral encephalitis or related injury (n=2). In four of the patients no resection and no pathological tissue were obtained. In two of these cases this was because of bilateral disease. In one case no resection was performed because of fear of injury to eloquent cortex. In the final situation the patient declined to continue forward with surgery. Seizure onset regions were most common in neocortical temporal structures, mesial temporal structures or a mix of the two (n=6). In two patients, seizures arose from frontal lobe structures (the cingulated gyrus or orbitofrontal regions). In three patients the seizures arose from the junction of the temporal, parietal and occipital lobes.

Seizure onset zones and seizure characteristics were determined independently from this research by a team of clinical electroencephalographers. Seizure type was determined by examination of the patient's ECoG recording, simultaneously recorded closed circuit video recordings of the patient's behavior, and clinical history of the patient. Seizures in which consciousness was impaired in any way were considered complex partial (CPS). Seizures which culminated in bilateral tonic, clonic or tonic-clonic movements and in which all or nearly all electrodes showed ictal activity were considered to have had secondary generalization. If awareness was maintained and the patient was able to interact appropriately the seizure was considered a simple partial seizure (SPS). Seizures which were ambiguous (e.g. brief events in which no interactions occurred with the patient before the seizure ended) were classified based on other events which had similar behavioral and electrographic features. Delineation of the seizure onset zone was made by observing which of the intracranial electrodes first showed ictal electrographic activity, including low voltage fast activity or repetitive spike-wave discharges. The initiation of the seizure as determined by this clinical team was used as the start of the seizure for purposes of the analysis discussed below. A count of the electrodes definitively involved in the onset of the typical seizure for a given patient is included in Table 1 as a reflection of focality. In all cases there was significant spread of ictal activity. The semiology and ECoG recordings of all patients involved focal features at onset. In 28 of 33 CPS, the ictal activity spread to include all or nearly all of the intracranial electrodes, while the ictal activity of SPS did not achieve complete electrographic generalization. In 7 of the 11 patients there was progression of at least one seizure to generalized tonic-clonic activity. In 3 of the patients the complex-partial seizures did not progress to such behavior, and in 1 patient only simple partial seizures occurred. Purely sub-clinical seizures were not included in this analysis.

We note that a potential concern in these data is the spatial spreading of electrical activity propagating through conductive tissue from a brain source to an electrode. To reach the scalp surface, electrical activity from a cortical source propagates through the cortex, cerebrospinal fluid, skull, and scalp. The result is significant spatial spreading (or blurring) of the original source voltage. For the ECoG data of interest here, this spreading is much less severe (Zaveri et al., 2009). As a result, we do not expect that passive voltage spread

will have significant effect on our results. If anything, the effect would be to increase overall levels of apparent synchronization. As described below, the results are the opposite of this.

Anatomical Figures

To create Figure 1A and the movie in the supplementary material, we used FreeSurfer (Dale et al., 1999) to reconstruct a 3D model of the cortical surface of the patient using pre-operative high resolution MRI data. We then co-registered this MRI data with a post-operative CT scan showing the location of the intracranial electrodes. We obtained each electrode coordinate manually from the post-operative CT scan and subsequently projected them onto the reconstructed 3D model of the cortex.

Calculation of functional topologies

Many different approaches exist to determine functional connectivity from time series data (Pereda et al., 2005). Different methods employ distinct coupling measures (e.g., linear or nonlinear measures) and different strategies for assigning network edges. In this work we focus on a simple measure of linear coupling: the cross correlation. We outline here our particular data analysis approach; a detailed discussion of the measure, including its statistical properties and simulation results, may be found in (Kramer et al., 2009). Before applying the coupling analysis, we process the ECoG data from each seizure and subject in the following way. First, we lowpass filter the data (third order Butterworth, zero-phase digital filtering) below 125 Hz, and notch filter (third order Butterworth, zero-phase digital filtering) the data at 60 Hz and 120 Hz. Then, to reduce the contribution to coupling of the reference electrode, we compute the average reference of the filtered data and subtract it from each electrode (Towle et al., 1999). Next, we divide the ECoG data into 1.024s windows with 0.512s overlap beginning 120s before seizure onset and ending 30s after seizure termination. Finally, we normalize the data from each electrode within the 1.024s window to have zero mean and unit variance.

With the data processed in this way, we construct a functional network for each (overlapping) ~1 s window. Our procedure for constructing functional networks from the data involves three steps. We briefly describe these steps here; again, a complete discussion may be found in (Kramer et al., 2009). In the first step we choose two electrodes, apply the cross correlation to the ECoG data, and select the maximum correlation within time delays of +/− 200 ms. Second, we determine the statistical significance of this correlation value through an analytic procedure that accounts for our choice of an extremum (Kramer et al., 2009). Third, we correct for multiple significance tests using a linear step-up procedure controlling the false detection rate (FDR) with $q=0.05$. For this choice of q, 5% of the network connections are expected to be falsely declared. The result is a network for each ~1 s window with an associated measure of uncertainty, namely the expected number of edges incorrectly declared present. Propagation of the network uncertainty to uncertainty in the network measures is nontrivial and the subject of future work.

We note that the rhythms dominating the ECoG data will also dominate the cross correlation measure we employ. Typically, these dominant rhythms occur in the low frequency bands, and we expect that the cross correlation measure will be most sensitive to this large amplitude, low frequency activity. To examine the networks that result in different frequency bands, we apply a separate coupling measure (the coherence) in the Supplementary Material. We find similar results for the networks produced by the cross correlation measure and the coherence measure in the low frequency bands, as expected (see Supplementary Material).

Analysis of topologies: graph theory and network measures

We illustrate the connectivity of the ECoG data as a network. In doing so we represent each electrode as a node and a sufficiently strong connection (defined as a statistically significant cross correlation) as an edge. The association measure we employ does not distinguish the direction of coupling and the resulting networks are therefore undirected. We choose to ignore the direction of coupling (determined by the lag of the maximum correlation) for two reasons. First, the cross correlation is a poor indicator of coupling direction for periodic time series. Second, we developed the statistical methods only to detect non-zero correlations (Kramer et al., 2009). To make inferences about more subtle aspects of the cross correlation, such as the sign, would require the development of a new measure and appropriate statistical tests. We show examples of the functional networks in Figures 1A,B. Our analysis focuses on how the network topologies evolve in time, in particular how these topologies change at seizure onset and during the course of a seizure.

To analyze the functional networks derived from the ECoG data, we apply five network measures: the density, the components, the similarity coefficient, and for the largest component the characteristic path length and clustering coefficient. We briefly define these measures here; more detailed descriptions may be found in (Wasserman and Faust, 1994; Newman, 2003; Kolaczyk, 2009). The *density* is the number of edges in the network divided by the total possible number of edges; for N nodes the total possible number of edges is N(N-1)/2. A density of 1 indicates an edge between each pair of nodes in the network. A *component* is a subset of nodes in which each node is reachable from every other node (i.e., following edges one can travel from each node in the component to any other node). A single node is a trivial component of size one. We monitor the largest component, number of components, and number of trivial components in the networks. The Jaccard *similarity coefficient* compares the edge sets of two networks and divides the size of their intersection by the size of their union. The similarity coefficient approaches 1 if two networks (with the same number of nodes) share a similar pattern of edges between their nodes. For the largest connected component we compute the *characteristic path length* (the number of edges traversed on average in traveling between pairs of nodes in the component) and the *clustering coefficient* (a measure of the cliquishness of a typical neighborhood (Watts and Strogatz, 1998)). Both measures only apply to the largest component in which paths between nodes are well defined. We note that each measure summarizes a topological characteristic of the entire network as a single scalar; we do not study the characteristics of individual nodes (e.g., their degree or betweenness centrality) here. Instead our goal is to summarize how the overall network topology evolves in time. In addition to the network measures, we also compute the signal energy of the ECoG data for each subject and seizure, and within each interval. To define the signal energy, we first lowpass filter the data (third order Butterworth, zero-phase digital filtering) below 125 Hz, and notch filter (third order Butterworth, zero-phase digital filtering) the data at 60 Hz and 120 Hz. Then we choose an interval (e.g., the first ictal interval, defined in the next subsection) and divide the data into ~1 s windows (with ~0.5 s overlap) that cover the interval. Next, for each 1 s window within the interval we compute the squared value of the (filtered) ECoG data at each electrode and average the results over the window (Litt et al., 2001). We then repeat this procedure for all intervals. Because we bandpass filter the ECoG data, the signal energy only captures activity within this frequency range.

Population summary measures

We applied the network topology measures to 48 seizures observed in 11 patients. Because seizure duration varies between seizures and subjects, we cannot summarize the population results by simply averaging in time. Instead, we normalize time for each subject and seizure by dividing the seizure duration into 10 intervals of equal length. We label these intervals I1,

I2,… I10. By normalizing time in this way, we assume that the seizures evolve in stereotypical ways that might occur more quickly or more slowly from subject to subject or even seizure to seizure. We have repeated the analysis using fixed time intervals of 10 s and find similar network topologies (Supplementary Figure 2). In addition to the ten ictal intervals, we also analyze the network properties in a preictal interval (labeled −1) that begins 120 s before seizure onset and ends 30 s before seizure onset. Similarly we define a postictal interval (labeled +1) that begins immediately at seizure termination and ends after three-tenths of the seizure duration (approximately 30 s).

To determine significant changes in the network measures and signal energy across the intervals for the entire collection of seizures we apply a one-way ANOVA blocked by patient (eleven levels) and with intervals (twelve levels) as the factor. We test the null hypothesis that samples at all interval levels are drawn from the same distribution. To determine which pairs of intervals exhibit significant differences in their means, we perform a multiple comparison procedure. We set $\alpha=0.05$ and use a critical value determined by Tukey's honestly significant difference criterion. In the figures we plot the network results for each interval averaged over the population of subjects and adjusted for differences in subjects. We identify a significant change in a network measure during the seizure only if the ictal values differ significantly from the preictal value.

RESULTS

Unlike the static structural networks based on anatomical connections between brain areas (Hilgetag and Kaiser, 2004; Sporns and Kötter, 2004; Bullmore and Sporns, 2009), we examine here dynamic, functional networks deduced from ECoG data. We determine these networks using a simple association measure: the cross correlation. We choose this measure for two main reasons: simple linear and sophisticated nonlinear measures appear to perform equally well when applied to ECoG data (Mormann et al., 2005; Ansari-Asl et al., 2006; Kreuz et al., 2007; Osterhage et al., 2007), and for the cross correlation we can derive an analytic and computationally efficient significance test (Kramer et al., 2009). Applying a frequency domain measure — the coherence — to the data produces similar results (Supplementary Material).

To construct functional networks from the ECoG data, we implement the following procedure. First we divide the ECoG data into ~1 s windows (with ~0.5 s overlap) beginning 120 s before seizure onset and ending after seizure termination. We choose this window size to preserve weak stationary in the data, but did find similar results with different window sizes and overlaps (Supplementary Material). We then compute the cross correlation — and test the significance — between all electrode pairs for the ECoG data within each window. Finally, we threshold the results of the significance tests to construct a functional network with an associated measure of uncertainty. A detailed discussion of the correlation measure and appropriate statistical tests may be found in (Kramer et al., 2009). We analyze these networks to show that while some properties (such as the overall level of network synchronization) are preserved during the seizure, others change dramatically.

Network synchronization decreases — while signal energy increases — during seizure progression

In Figure 1 we show example networks constructed from the ECoG data. While the data can be displayed on a 3-dimensional reconstruction of the cortical surface (Figure 1A) it is more useful to show these data as a circular network; each subject had electrodes which entered the cortical surface and therefore remain hidden in the cortical surface reconstructions. Accordingly, to observe the connectivity of the entire network, we arrange the electrodes in a ring and connect electrodes exhibiting significant coupling with an edge (i.e., a

directionless link between nodes). Figure 1A and B suggest an obvious way in which the network topologies change in time; there is a dramatic variation in the number of edges (a movie illustrating this variation in another subject is provided in the Supplementary Material). In this example, at seizure onset and termination the networks possess many more edges (i.e., become more synchronized) than during the middle portion of the seizure. To quantify the changing number of edges observed, we compute the density of each network. This measure ranges from 0 (a desynchronized network containing no edges) to 1 (a hypersynchronized network with edges connecting all possible pairs of nodes). In this example, the density increases briefly just after ictal onset, decreases to preictal values during the ictus itself, and again increases before seizure termination (Figure 1C). For comparison, we also show the simultaneous ECoG activity recorded at a single electrode, and for three, two -second intervals from multiple electrodes for this seizure (Figure 1C). Surprisingly, the large amplitude voltage oscillations characteristic of a seizure occur after the density returns to preictal levels.

To quantify the changing voltage dynamics and network synchronization during the seizure, we analyze an ensemble of 48 seizures collected from 11 patients. We first normalize time for each seizure by dividing the ictal period into ten intervals of equal length. In doing so, we assume that seizures undergo characteristic progressions that can be stretched or compressed in time; repeating the analysis with time intervals of fixed duration and different seizure lengths produces similar results (Supplementary Figure 2). We then compute the density for all subjects and seizures within preictal, ictal, and postictal intervals and plot the average density per interval adjusted for differences in subjects with a blocked one-way ANOVA (Figure 1D). Only after ictal onset (interval label I1) and before termination (I9, I10) do we observe a significant increase in density above preictal levels during the seizure (see Methods). During the middle portion of the seizure (intervals I2-I8) the density returns to preictal levels. We find similar changes in density for a subset of 10 patients with focal seizure onsets (i.e., all patients except Patient *F* in Table 1), and for subsets of patients and seizures grouped by seizure type (Supplementary Figure 1). We also show in Figure 1D the signal energy (see Methods) within each interval adjusted for patient differences. In contrast to the density, we find a significant increase in overall signal energy for all ictal and postictal intervals compared to the preictal level. The increase in signal energy is not surprising; seizure activity typically manifests as large amplitude voltage oscillations at the macroscopic spatial scale recorded in the ECoG or EEG (electroencephalogram). To support these large amplitude oscillations, we expect increased synchrony at the microscopic spatial scale of individual neurons. Although increased synchrony at the microscopic spatial scale supports the large amplitude ECoG rhythms, we find that synchrony decreases (i.e., density decreases) between macroscopic brain areas during seizure.

The network topology and signal energy also change dramatically at seizure termination. The density increases substantially in the postictal interval compared to preictal or ictal values, while the voltage fluctuations decrease. A low amplitude, slow wave rhythm (visible in Figure 1C) that appears broadly throughout the brain dominates the postictal activity and contributes to the increased network density. Low frequency rhythms often appear in the postical period (Kaibara and Blume, 1988), although the exact mechanisms that support this activity are unknown (Fisher and Schachter, 2000). We note that the density increase begins before seizure termination (see I9 and I10 of Figure 1D), consistent with previous observations of increased synchrony in the late seizure stage (Topolnik et al., 2003; Schindler et al., 2007).

Dominant networks fracture, then reform, during seizure propagation

Although the voltage dynamics change dramatically during the seizure, our first measure of the network topology — the density — does not. Perhaps the ictal networks change in more

subtle ways, reorganizing, rather than trimming or growing, their edges? To address this possibility, we examine the network components within each interval. Briefly, a component is a connected subnetwork of mutually reachable nodes (i.e., any node in the component can reach any other node in the same component by following a sequence of edges). The average number of nontrivial components — components that consist of two or more nodes — adjusted for differences in subjects increases significantly (see Methods) during the middle portion of the seizures (Figure 2A).

Thus, as the density returns to preictal levels during the seizure (intervals I2-I8 in Figure 1C), more nontrivial components emerge. Does one connected subnetwork dominate and contain most of the nodes? Or, are the nodes more evenly distributed between smaller subnetworks? To investigate this, we determine the percentage of nodes within each of the components for the ensemble of seizures (Figure 2B). At ictal onset, nearly half of all nodes reside in the largest component, which therefore dominates the network. As the seizure progresses, the largest component fractures — nodes “leave” this component and become isolated or form other, smaller subnetworks. Finally, just before seizure termination, a majority of nodes rejoin to establish a single dominant component.

We illustrate the fracturing and reforming of the largest subnetwork for a single subject and seizure in Figure 2C. At ictal onset (I1), a majority of nodes join the largest component which here covers portions of the frontal, parietal, and temporal lobes — almost the entire extent of the lateral neocortex as well as subcortical brain regions. During the seizure (I6, middle row), the largest component shrinks and collections of nontrivial components emerge. Finally, at ictal termination (I10, bottom row) nodes rejoin the giant component which again dominates the network. In this example, and for the population of subjects, the ictal subnetworks merge at onset, fracture during seizure, and rejoin just before termination.

Small-world topologies of the largest subnetwork emerge during preictal and ictal intervals

The largest subnetworks, which incorporate between 30% and 60% of the nodes during the seizure, play a prominent role in the network topology. To examine the properties of these dominant subnetworks, we determine the characteristic path length and clustering coefficient for the largest component of each network. Because the size of the largest subnetwork changes in time (as nodes break-off and re-join the dominant component) we scale the observed values by those expected for a one-dimensional lattice with the same number of nodes and average degree (Watts and Strogatz, 1998). We find that the (scaled) characteristic path lengths in the observed networks remain less than one for all intervals, while the (scaled) clustering coefficients tend to exceed one during seizure (Figure 3). Combined, these results suggest that, for most of the seizure, the largest preictal and ictal subnetworks exhibit small-world topologies (greater clustering coefficients yet smaller path lengths than the associated one-dimensional lattices) for all examined intervals (Netoff et al., 2004; Ponten et al., 2007). Although the ictal subnetworks exhibit small-world topologies, the properties of these topologies evolve in time. Just after seizure onset (I3), both the path length and clustering coefficient tend to increase (the former increases significantly), and the networks move in the direction of becoming a more regular lattice with mesh-like connections between nodes, in agreement with previously reported observations near seizure onset (Ponten et al., 2007; Schindler et al., 2008). Just before seizure termination (I10), the (scaled) path lengths and clustering coefficients decrease dramatically, suggesting the networks evolve towards a more random configuration, as observed in (Schindler et al., 2008).

Network topologies become more similar during — and between — seizures

Most patients with epilepsy experience seizures with clinical manifestations (e.g., stereotyped motions) that are similar across seizures within an individual. The voltage activity observed during seizures also appears stereotyped. To determine whether the networks that appear during the seizure do so in stereotyped ways, we apply two measures focused on different aspects of the topological similarities (Figure 4A). The top two rows show example networks extracted from the preictal interval (label −1) and a middle ictal interval (label I6) from a single seizure and subject. The bottom two rows show another set of networks extracted from the same subject and intervals but from a different seizure. Visual inspection suggests more variability in the preictal networks over time. In addition, the ictal networks appear roughly consistent in the two seizures; notice, for example, the concentration of edges in the lower left regions of the networks.

We quantify these observations with two measures. The first — the intra-seizure similarity — examines the variability of networks within a fixed interval of a chosen seizure. To compute this measure we compare each network within an interval (i.e., within interval “-1” of the first seizure of a chosen subject) to all other networks within the same interval and seizure. The intra-seizure similarity is large when the variability in the networks within the interval is small. We apply the intra-seizure similarity measure to each interval for all subjects and seizures, and plot the average results for each interval (adjusting for differences in subjects) in Figure 4B. During seizure (intervals I1 to I9) the intra-seizure similarity increases significantly (see Methods) compared to preictal values; ictal topologies within each interval become more similar (or exhibit less variability) than the preictal networks. We note the dramatic decrease in similarity during the postictal interval. Although large subnetworks dominate this period (Figure 2B), the topologies of these networks exhibit high variability.

To determine the consistency of networks between seizures, we apply a second measure: the inter-seizure similarity (see Methods). In this measure we choose an interval (e.g., “−1”) and compare networks from the same interval and subject across different seizures. For example, we compare each network in the first and third rows (or second and forth rows) of Figure 4A. We repeat this procedure for each patient and note that all patients studied here had at least two seizures. Compared to the intra-seizure similarity, the inter-seizure measure is smaller (Figure 4B); we expect more variability (and less topological consistency) between different seizures of a subject. Yet, we observe that ictal networks in early and middle intervals become significantly more similar than preictal networks from seizure-to-seizure. We conclude that similar ictal networks appear from seizure-to-seizure for a patient, and in that sense the network topologies that emerge, like the voltage rhythms, are consistent.

DISCUSSION

Consistent topological changes during the seizures and implications for hypersynchrony

We have explored the dynamic topologies of cortical and subcortical functional networks during human epileptic seizures. Although these seizures resulted from multiple different etiologies, were recorded from different cortical and subcortical locations, and included both complex and simple partial seizures, we found remarkable consistency in the evolution of network structure during the seizure. Convention would suggest that the dramatic voltage oscillations characteristic of seizures correlate with hypersynchronous functional networks (i.e., networks with many edges or high density). Surprisingly, the onset of large amplitude voltage oscillations does not affect the network density. Instead, networks were no more synchronous in the middle of the seizure than preictally (i.e., acquired no more edges). This suggests that seizures are not uniformly hypersynchronous states — at least not at the level

of large neuronal populations. Instead, synchrony is largest at ictal onset and termination, and evolves in time. These results are consistent with previous reports of an increase in coupling near seizure onset (following a rapid discharge) (Wendling et al., 2001, 2003; Bartolomei et al., 2004; Ponten et al., 2007; Arthuis et al., 2009) and subsequent desynchronization during large amplitude, low frequency oscillations characteristic of seizure progression (Schindler et al., 2007, 2008). We note that the spatial scale of measurement is critical here. At the microscopic scale of individual neurons we expect increased synchrony in small regions to generate the large amplitude voltage oscillations observed at an individual electrode (e.g, Figure 1C). Yet, at the macroscopic spatial scale, we observe decreased synchrony between electrodes (i.e., between macroscopic brain regions). Relating dynamics and synchrony between these spatial scales remains a crucial question.

Overall network synchronization provides a crude characterization of network topology. To explore the detailed network structure, we applied a variety of analysis techniques that revealed stereotyped patterns of network evolution from seizure onset to termination. At seizure onset, a large subnetwork of connected nodes emerged. This dominant component then fractured into smaller subnetworks. Approaching seizure termination, these subnetworks rejoined to again establish a dominant network component. Throughout the seizure, the largest component always exhibited a small-world topology. Yet, this structure varied, becoming more regular (i.e., more like a structure with mesh-like connections between neighboring nodes) during the seizure and more random just before seizure termination.

Consistent topologies emerged between seizures in an individual. Specifically, each individual subject produced similar networks consistent from seizure to seizure. This result coincides with the clinical observation that an individual's seizures are stereotypical events with reproducible patterns of initiation and spread (Gibbs et al., 1937; Litt et al., 2001). In addition, we observed that seizures from heterogeneous etiologies (Table 1) resulted in similar topological progressions from seizure onset to termination, consistent with seizure progression through specific clinical stages (from aura to focal event to generalized event to postictal period), rhythmic stages (from very fast oscillations to large amplitude, slowing rhythms to bursting to silence), and the more general stages of initiation, propagation and termination (Pinto et al., 2005).

The similarity of topological evolution across heterogeneous etiologies bolsters the idea that the seizure is a unifying event - a final common pathway from a number of insults - and suggests that the biophysical mechanisms for seizure initiation and propagation are relatively conserved. Many different seizure types seem to share common cellular and network mechanisms (McCormick and Contreras, 2001) and we would like to understand the rhythmic and topological evolution of seizures in terms of specific biological mechanisms (e.g., in terms of neural discharges (Traub et al., 1996), evolving afterdischarges (Trevelyan et al., 2007), depolarizariation block of interneurons (Ziburkus et al., 2006), depression of excitatory postsynaptic potentials (Nita et al., 2008), or homeostatic synaptic plasticity (Houweling et al., 2005)). Simulation studies (Netoff et al., 2004; Dyhrfjeld-Johnsen et al., 2007; Lytton, 2008; Bogaard et al., 2009) and multiscalar observations combining single neuron recordings (microscale), local field potentials (mesoscale) and macroscopic ECoG, may help uncover this relationship between dynamic network activity and its underlying mechanisms.

To summarize the network evolution we emphasized measures that condensed important network features to single scalar values (e.g., the network density or number of components). These reductions of the complex network data facilitated a straightforward

comparison of network attributes across the patient population. Although useful, the reductions prohibit a detailed analysis of the focal network features of individual nodes. Concentrating on these focal characteristics may serve an important role in examining the patterns of activity that emerge during seizure propagation (e.g., spiral waves (Huang et al., 2004)). In addition, such focal measures may assist in seizure localization and treatment, for example in identifying brain regions that act as “hubs” of seizure activity (Morgan and Soltesz, 2008; Kramer et al., 2008).

Topological and dynamical changes affecting seizure termination

Increasing density and growth of the largest component suggest more synchronization near seizure termination, consistent with recent observations (Topolnik et al., 2003; Schiff et al., 2005; Schindler et al., 2007, 2008). In addition, we observe that the topology of the largest network component evolves towards a more random configuration just before seizure termination, in agreement with (Schindler et al., 2008). These topological changes occur as the ECoG dynamics develop bursts — brief intervals of large amplitude voltage activity interspersed with longer intervals of low amplitude fluctuations — near seizure termination. Modeling studies show that random network topologies support bursting dynamics (Netoff et al., 2004) and better synchronize their dynamics than more regular network organizations (Chavez et al., 2006). In addition, *in vitro* observations reveal that bursting dynamics are more synchronous than ictal dynamics (Netoff and Schiff, 2002). We might therefore envision a positive feedback loop between the network topology and bursting dynamics that ends the seizure. As the seizure approaches termination, the networks acquire more random configurations and therefore might better synchronize their bursting dynamics. This increased synchronization results in more network edges which act to synchronize the dynamics even more. Eventually, enough edges unite the fractured subnetworks and the bursting dynamics cease. Unraveling the relationship between network topology and dynamics will provide insights into not only epilepsy but perhaps into the dynamics of complex networks in general (Gross and Blasius, 2008).

Ideally, we seek a complete spatiotemporal understanding of the entire ictal event. Such a characterization would incorporate the rhythmic patterns that emerge in the voltage activity during the seizure (e.g., high frequency oscillations (Allen et al., 1992; Alarcon et al., 1995; Roopun et al., 2009), ictal chirps (Schiff et al., 2000), and spike wave complexes (Gibbs et al., 1937)) with the spatial network characteristics. How to unify these rhythmic patterns (observed in ECoG or scalp EEG data recorded at individual electrodes) with the network topologies (observed across multiple electrodes) and pathological brain functioning remains an open challenge.

Implications for epilepsy therapies

The current mainstay of epilepsy treatment continues to be medications with surgical treatments a last resort reserved for patients with pharmaco-resistant epilepsy. Unfortunately, surgical treatment of epilepsy has only limited effectiveness. It is estimated that, overall, surgery only helps 60–70% of patients with intractable seizures. Newer approaches include stimulation of cortex in response to seizure activity (Morrell, 2006). The results reported here suggest a variety of alternatives for surgical manipulation and electrical stimulation treatments responsive to the network topologies. Because the ictal networks evolve in time, the treatment strategies employed may depend on the time of intervention. For example, it may be maximally efficient to prevent the formation of the largest component at onset through desynchronization (i.e., to prevent the increases in density observed at ictal onset). A more innovative technique would be a stimulation designed to assist in reformation of the large component after its fracturing; we note that the largest amplitude pathological voltage oscillations characteristic of a seizure occur during this

fracturing period. Perhaps appropriate electrical stimulation could prevent the march through network fracturing and lead to a rapid cessation of the seizure without clinical manifestations. A disadvantage of this proposed intervention is that it follows seizure initiation; to serve as an effective therapeutic target, the network fracturing must still precede the clinical manifestation of the seizure (e.g., loss of awareness). An advantage of this temporally focused approach is that no requirement for seizure prediction or anticipation would be necessary.

More fundamentally, the results presented here bolster a growing literature which is forcing us to reconsider the textbook description of seizures as hypersynchronous events. This realization and accompanying detailed, quantitative description of seizure dynamics may permit entirely new methods of seizure control.

Supplementary Material

Refer to Web version on PubMed Central for supplementary material.

Acknowledgments

The authors would like to thank Matt Bianchi, Corey Keller, Caroline Raclin, M. O. Shafi, Kevin Staley and M. Brandon Westover for comments on early versions of this manuscript, Hemant Bokil for assistance implementing the coherence analysis, and Alex Chan and Andrew Dykstra for assistance in visualization of the data as well as comments on the manuscript. MAK holds a Career Award at the Scientific Interface from the Burroughs Wellcome Fund. UTE acknowledges support by the National Science Foundation under grant number IIS-0643995. EDK acknowledges support by ONR award N00014-06-1-0096. EE was supported by: NEI R01EY017658, NIDA R01NS063249, NSF IOB 0645886, the Howard Hughes Medical Institute, and the Klingenstein Foundation. SSC was supported by funds from an American Epilepsy Foundation - Grass - Morison Fellowship, the Rappaport Foundation and NINDS R01 NS062092

References

Alarcon G, Binnie CD, Elwes RD, Polkey CE. Power spectrum and intracranial EEG patterns at seizure onset in partial epilepsy. Electroenceph Clin Neurophysiol 1995;94:326–337. [PubMed: 7774519]

Allen PJ, Fish DR, Smith SJ. Very high-frequency rhythmic activity during SEEG suppression in frontal lobe epilepsy. Electroenceph Clin Neurophysiol 1992;82:155–159. [PubMed: 1370786]

Ansari-Asl K, Senhadji L, Bellanger JJ, Wendling F. Quantitative evaluation of linear and nonlinear methods characterizing interdependencies between brain signals. Phys Rev E 2006;74:031916.

Arthuis M, Valton L, Régis J, Chauvel P, Wendling F, Naccache L, Bernard C, Bartolomei F. Impaired consciousness during temporal lobe seizures is related to increased long-distance cortical-subcortical synchronization. Brain 2009;132:2091–2101. [PubMed: 19416952]

Bartolomei F, Wendling F, Régis J, Gavaret M, Guye M, Chauvel P. Pre-ictal synchronicity in limbic networks of mesial temporal lobe epilepsy. Epilepsy Res 2004;61:89–104. [PubMed: 15451011]

Bartolomei F, Wendling F, Vignal JP, Kochen S, Bellanger JJ, Badier JM, Bouquin-Jeannes RL, Chauvel P. Seizures of temporal lobe epilepsy: identification of subtypes by coherence analysis using stereo-electro-encephalography. Clin Neurophysiol 1999;110:1741–1754. [PubMed: 10574289]

Bogaard A, Parent J, Zochowski M, Booth V. Interaction of cellular and network mechanisms in spatiotemporal pattern formation in neuronal networks. J Neurosci 2009;29:1677–1687. [PubMed: 19211875]

Brazier, MA. Electrical seizure discharge within the humn brain: the problem of spread. In: Brazier, MA., editor. Epilepsy, its phenomenon in man, chapter Electrical seizure discharge within the humn brain: the problem of spread. Academic Press; 1973.

Bullmore E, Sporns O. Complex brain networks: graph theoretical analysis of structural and functional systems. Nat Rev Neurosci 2009;10:186–198. [PubMed: 19190637]

Chavez M, Hwang D, Amann A, Boccaletti S. Synchronizing weighted complex networks. Chaos 2006;16:015106. [PubMed: 16599772]

Dale AM, Fischl B, Sereno MI. Cortical surface-based analysis. I. Segmentation and surface reconstruction. Neuroimage 1999;9:179–194. [PubMed: 9931268]

Dyhrfjeld-Johnsen J, Santhakumar V, Morgan RJ, Huerta R, Tsimring L, Soltesz I. Topological determinants of epileptogenesis in large-scale structural and functional models of the dentate gyrus derived from experimental data. J Neurophysiol 2007;97:1566–1587. [PubMed: 17093119]

Ferri R, Stam CJ, Lanuzza B, Cosentino FII, Elia M, Musumeci SA, Pennisi G. Different EEG frequency band synchronization during nocturnal frontal lobe seizures. Clin Neurophysiol 2004;115:1202–1211. [PubMed: 15066546]

Fisher RS, Schachter SC. The Postictal State: A Neglected Entity in the Management of Epilepsy. Epilepsy Behav 2000;1:52–59. [PubMed: 12609127]

Gibbs F, Gibbs E, Lennox W. Epilepsy: a paroxysmal cerebral dysrhythmia. Brain 1937;60:377–388.

Gotman J. Measurement of small time differences between EEG channels: method and application to epileptic seizure propagation. Electroenceph Clin Neurophysiol 1983;56:501–514. [PubMed: 6194969]

Gross T, Blasius B. Adaptive coevolutionary networks: a review. J Roy Soc Interface 2008;5:259–271. [PubMed: 17971320]

Guye M, Régis J, Tamura M, Wendling F, McGonigal A, Chauvel P, Bartolomei F. The role of corticothalamic coupling in human temporal lobe epilepsy. Brain 2006;129:1917–1928. [PubMed: 16760199]

Hilgetag CC, Kaiser M. Clustered organization of cortical connectivity. Neuroinformatics 2004;2:353–360. [PubMed: 15365196]

Houweling AR, Bazhenov M, Timofeev I, Steriade M, Sejnowski TJ. Homeostatic synaptic plasticity can explain post-traumatic epileptogenesis in chronically isolated neocortex. Cereb Cortex 2005;15:834–845. [PubMed: 15483049]

Huang X, Troy WC, Yang Q, Ma H, Laing CR, Schiff SJ, Wu JY. Spiral waves in disinhibited mammalian neocortex. J Neurosci 2004;24(44):9897–9902. [PubMed: 15525774]

Jerger KK, Weinstein SL, Sauer T, Schiff SJ. Multivariate linear discrimination of seizures. Clin Neurophysiol 2005;116:545–551. [PubMed: 15721068]

Kaibara M, Blume WT. The postictal electroencephalogram. Electroenceph Clin Neurophysiol 1998;70:99–104. [PubMed: 2456198]

Kolaczyk, ED. Statistical Analysis of Network Data: Methods and Models. Springer; 2009.

Kramer MA, Eden UT, Cash SS, Kolaczyk ED. Network inference with confidence from multivariate time series. Phys Rev E 2009;79:061916.

Kramer MA, Kolaczyk ED, Kirsch HE. Emergent network topology at seizure onset in humans. Epilepsy Res 2008;79:173–186. [PubMed: 18359200]

Kreuz T, Mormann F, Andrzejak RG, Kraskov A, Lehnertz K, Grassberger P. Measuring synchronization in coupled model systems: A comparison of different approaches. Physica D 2007;225:29–42.

Litt B, Esteller R, Echauz J, D'Alessandro M, Shor R, Henry T, Pennell P, Epstein C, Bakay R, Dichter M, Vachtsevanos G. Epileptic seizures may begin hours in advance of clinical onset: a report of five patients. Neuron 2001;30:51–64. [PubMed: 11343644]

Lytton WW. Computer modelling of epilepsy. Nat Rev Neurosci 2008;9:626–637. [PubMed: 18594562]

McCormick DA, Contreras D. On the cellular and network bases of epileptic seizures. Ann Rev Physiol 2001;63:815–846. [PubMed: 11181977]

Morgan RJ, Soltesz I. Nonrandom connectivity of the epileptic dentate gyrus predicts a major role for neuronal hubs in seizures. Proc Natl Acad Sci USA 2008;105:6179–6184. [PubMed: 18375756]

Mormann F, Kreuz T, Rieke C, Andrzejak RG, Kraskov A, David P, Elger CE, Lehnertz K. On the predictability of epileptic seizures. Clin Neurophysiol 2005;116:569–587. [PubMed: 15721071]

Morrell M. Brain stimulation for epilepsy: can scheduled or responsive neurostimulation stop seizures? Curr Opin Neurol 2006;19:164–168. [PubMed: 16538091]

Netoff TI, Clewley R, Arno S, Keck T, White JA. Epilepsy in small-world networks. J Neurosci 2004;24:8075–8083. [PubMed: 15371508]

Netoff TI, Schiff SJ. Decreased neuronal synchronization during experimental seizures. J Neurosci 2002;22:7297–7307. [PubMed: 12177225]

Newman M. The structure and function of complex networks. SIAM Review 2003;45:167.

Nita DA, Cissé Y, Timofeev I. EPSP depression following neocortical seizures in cat. Epilepsia 2008;49:705–709. [PubMed: 18031546]

Osterhage H, Mormann F, Staniek M. Measuring synchronization in the epileptic brain: a comparison of different approaches. Int J Bifurcat Chaos 2007;17:3539–3544.

Penfield, W.; Jasper, H. Epilepsy and the Functional Anatomy of the Human Brain. Little Brown and Co; 1954.

Pereda E, Quiroga R, Bhattacharya J. Nonlinear multivariate analysis of neurophysiological signals. Prog Neurobiol 2005;77:1–37. [PubMed: 16289760]

Pinto DJ, Patrick SL, Huang WC, Connors BW. Initiation, propagation, and termination of epileptiform activity in rodent neocortex in vitro involve distinct mechanisms. J Neurosci 2005;25:8131–8140. [PubMed: 16148221]

Ponten SC, Bartolomei F, Stam CJ. Small-world networks and epilepsy: graph theoretical analysis of intracerebrally recorded mesial temporal lobe seizures. Clin Neurophysiol 2007;118:918–927. [PubMed: 17314065]

Reijneveld JC, Ponten SC, Berendse HW, Stam CJ. The application of graph theoretical analysis to complex networks in the brain. Clin Neurophysiol 2007;118:2317–2331. [PubMed: 17900977]

Roopun AK, Traub RD, Baldeweg T, Cunningham MO, Whittaker RG, Trevelyan A, Duncan R, Russell AJC, Whittington MA. Detecting seizure origin using basic, multiscale population dynamic measures: preliminary findings. Epilepsy and Behavior 2009;14 Suppl 1:39–46. [PubMed: 18834957]

Schiff SJ, Colella D, Jacyna GM, Hughes E, Creekmore JW, Marshall A, Bozek-Kuzmicki M, Benke G, Gaillard WD, Conry J, Weinstein SR. Brain chirps: spectrographic signatures of epileptic seizures. Clin Neurophysiol 2000;111:953–958. [PubMed: 10825700]

Schiff SJ, Sauer T, Kumar R, Weinstein SL. Neuronal spatiotemporal pattern discrimination: the dynamical evolution of seizures. Neuroimage 2005;28:1043–1055. [PubMed: 16198127]

Schindler K, Bialonski S, Horstmann MT, Elger C, Lehnertz K. Evolving functional network properties and synchronizability during human epileptic seizures. Chaos 2008;18 033119-6.

Schindler K, Leung H, Elger CE, Lehnertz K. Assessing seizure dynamics by analysing the correlation structure of multichannel intracranial EEG. Brain 2007;130:65–77. [PubMed: 17082199]

Sporns O, Kötter R. Motifs in brain networks. PLoS Biol 2004;2:e369. [PubMed: 15510229]

Topolnik L, Steriade M, Timofeev I. Partial cortical deafferentation promotes development of paroxysmal activity. Cereb Cortex 2003;13:883–893. [PubMed: 12853375]

Towle VL, Carder RK, Khorasani L, Lindberg D. Electrocorticographic coherence patterns. J Clin Neurophysiol 1999;16:528–547. [PubMed: 10600021]

Traub RD, Borck C, Colling SB, Jefferys JG. On the structure of ictal events in vitro. Epilepsia 1996;37:879–891. [PubMed: 8814102]

Trevelyan AJ, Baldeweg T, van Drongelen W, Yuste R, Whittington M. The source of afterdischarge activity in neocortical tonic-clonic epilepsy. J Neurosci 2007;27:13513–13519. [PubMed: 18057209]

Wasserman, S.; Faust, K. Social Network Analysis: Methods and Applications. Cambridge University Press; 1994.

Watts DJ, Strogatz SH. Collective dynamics of small-world networks. Nature 1998;393:440–442. [PubMed: 9623998]

Wendling F, Bartolomei F, Bellanger JJ, Bourien J, Chauvel P. Epileptic fast intracerebral EEG activity: evidence for spatial decorrelation at seizure onset. Brain 2003;126:1449–1459. [PubMed: 12764064]

Wendling F, Bartolomei F, Bellanger JJ, Chauvel P. Interpretation of interdependencies in epileptic signals using a macroscopic physiological model of the EEG. Clin Neurophysiol 2001;112:1201–1218. [PubMed: 11516732]

Zaveri HP, Duckrow RB, Spencer SS. Concerning the observation of an electrical potential at a distance from an intracranial electrode contact. Clin Neurophysiol 2009;120:1873–1875. [PubMed: 19748311]

Ziburkus J, Cressman JR, Barreto E, Schiff SJ. Interneuron and pyramidal cell interplay during in vitro seizure-like events. J Neurophysiol 2006;95:3948–3954. [PubMed: 16554499]

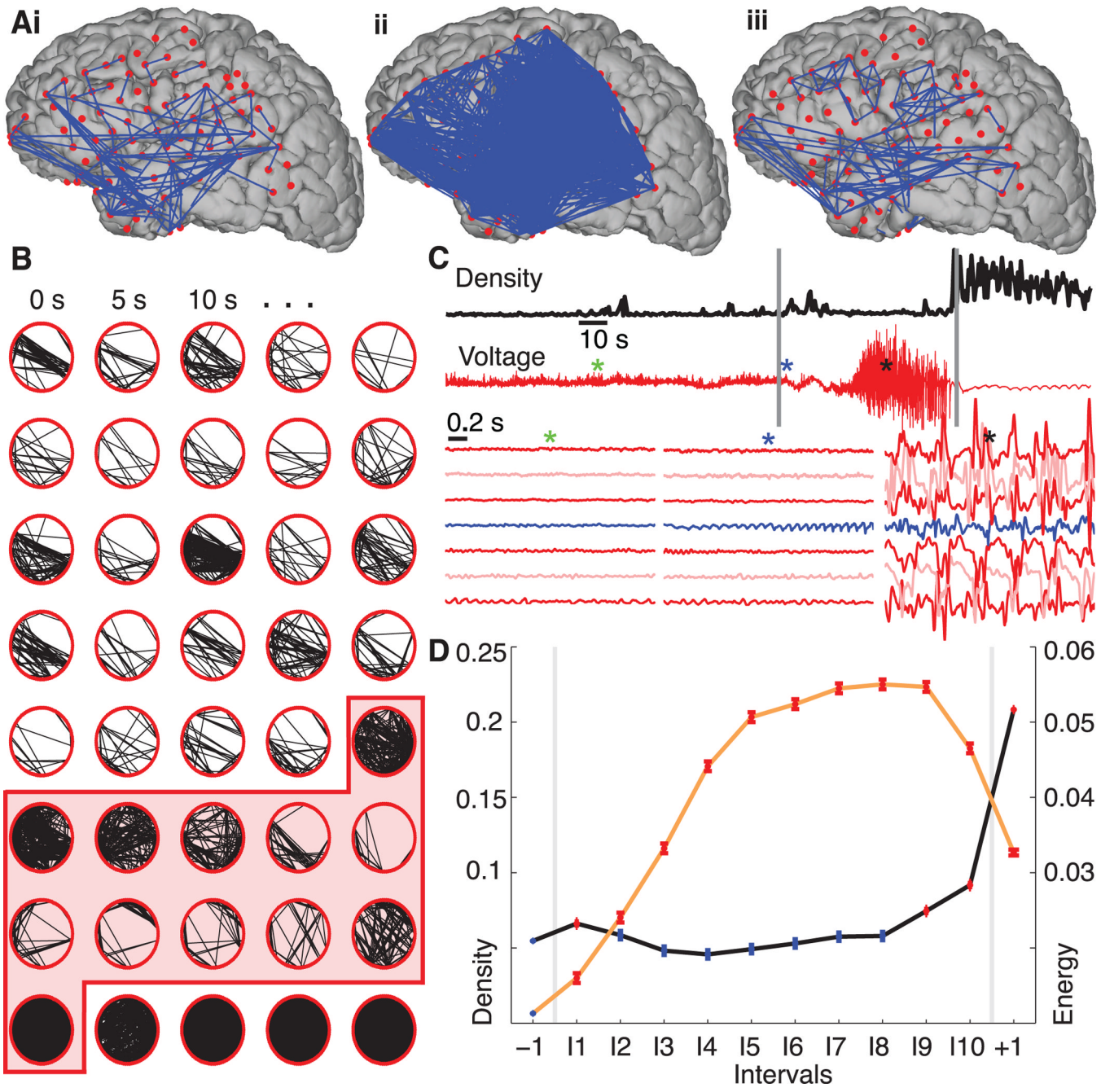

Figure 1.

Network synchronization increases at ictal onset and offset, but falls to preictal values during the seizure. **(A)** Representative networks just before the seizure starts (i), at seizure initiation (ii), and in the middle of the seizure (iii) from a single seizure in a single patient. In this example the electrode locations have been projected onto a reconstruction of this patient's cortical surface. Because some of the electrodes can not be easily visualized in this 2-dimensional representation, the data are displayed as circular networks containing all electrodes as individual nodes. **(B)** The networks progress from left to right, top to bottom, with a 2.5 s interval between networks. We arrange the 97 electrodes in a circle (without reference to their physical locations) and indicate sufficiently strong coupling between

electrode pairs with black lines. The shaded region denotes the ictal interval. Visual inspection of the evolving network topologies suggests increased network density (i.e., more edges) near ictal onset and termination. **(C)** The network density (black) and ECoG data from a single electrode (red, upper) for the representative example. At ictal onset and termination, indicated with the vertical gray lines, the network density increases dramatically, while during the middle portion of the seizure the ECoG data exhibits large amplitude fluctuations. The colored asterisks indicate the location of three, 2s intervals plotted for representative grid and strip electrodes below, including the activity of the presumptive onset electrode as identified by the clinical team (blue trace). **(D)** The density (black curve) — averaged across all subjects and seizures and adjusted for differences in subjects — for 12 time intervals: one preictal −1, ten ictal I1,I2,…,I10, and one postictal +1. In each interval, the circle indicates the mean density (n=9049 networks preictal, n=939 networks per ictal interval, and n=2817 networks postictal) and the vertical lines the standard error. Statistically significant increases in density compared to preictal values (see Methods) are indicated in red and occur at ictal onset (interval I1) and near ictal offset (intervals I9, I10, +1). We also plot the normalized signal energy (orange curve) for each interval averaged across all subjects and seizures (n=45609 preictal, n=3614 per ictal interval, and n=10842 postictal). Unlike the density, the signal energy increases significantly above preictal values for all ictal and postictal intervals.

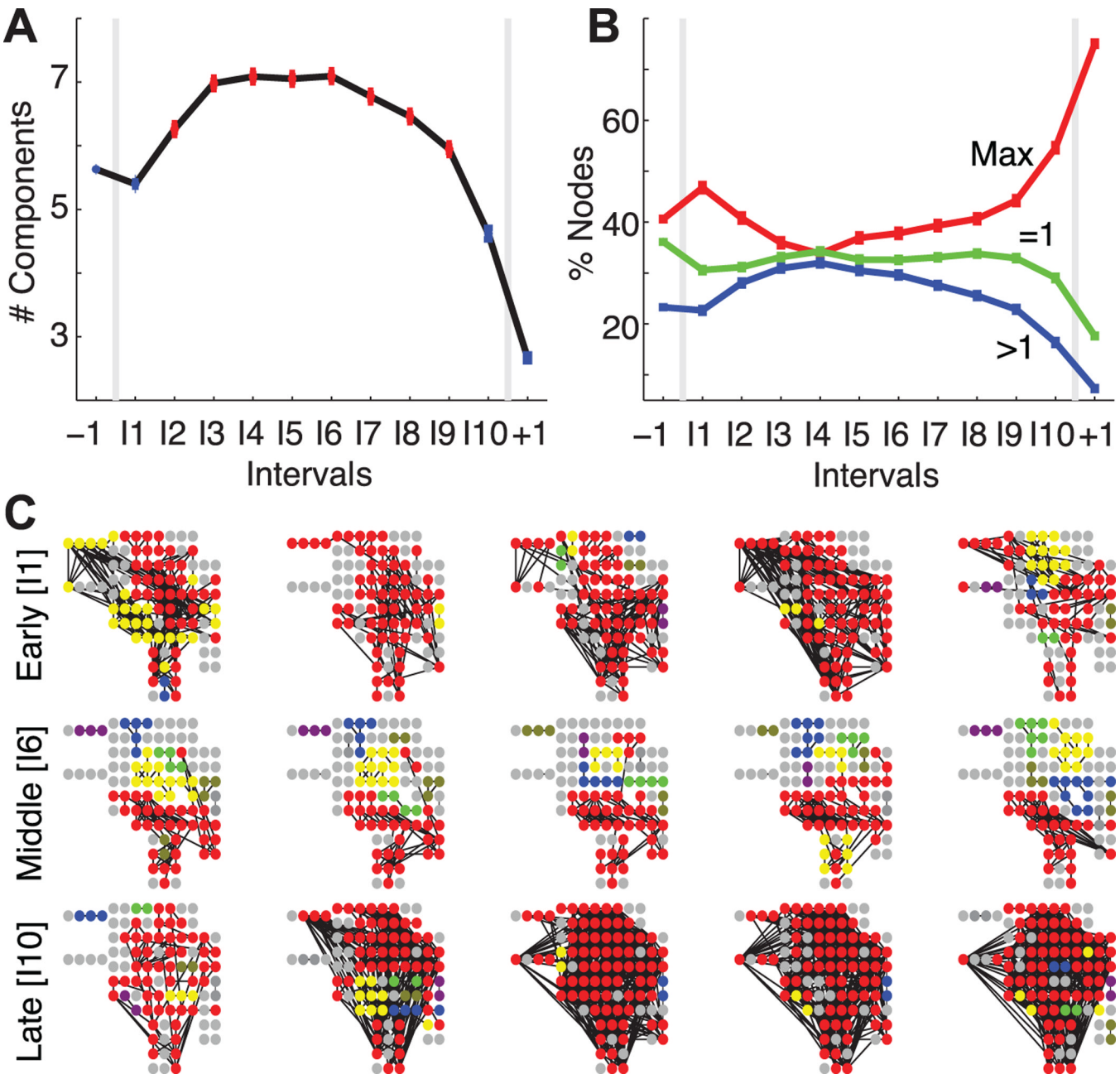

Figure 2.

The largest network components fracture during the seizure. **(A)** The average number of connected components (adjusted for differences in subjects) increases during the course of a seizure; points plotted in red indicate a statistically significant increase from the preictal value (number of networks per interval same as in Figure 1, see Methods). **(B)** The average percentage of nodes in the largest connected component (red, Max label), in trivial components (green, =1 label), and in other connected components (blue, >1 label) for the population of subjects and adjusted for differences in subjects. After ictal onset, nodes leave the largest component and become isolated or join other connected components. **(C)** Examples of connected components during early ictal (top row), middle ictal (middle row), and late ictal (bottom row) intervals for a single subject and seizure. Each circle indicates an

electrode (including both those on the cortical surface or subcortical) oriented to match surgical placement, and each black line indicates an edge. The electrode colors signify components — all electrodes of the same color belong to the same component, red denotes the largest component, and gray denotes single (isolated) electrodes. During the middle seizure interval, the largest component shrinks as more non-trivial components appear compared to the early and late ictal intervals.

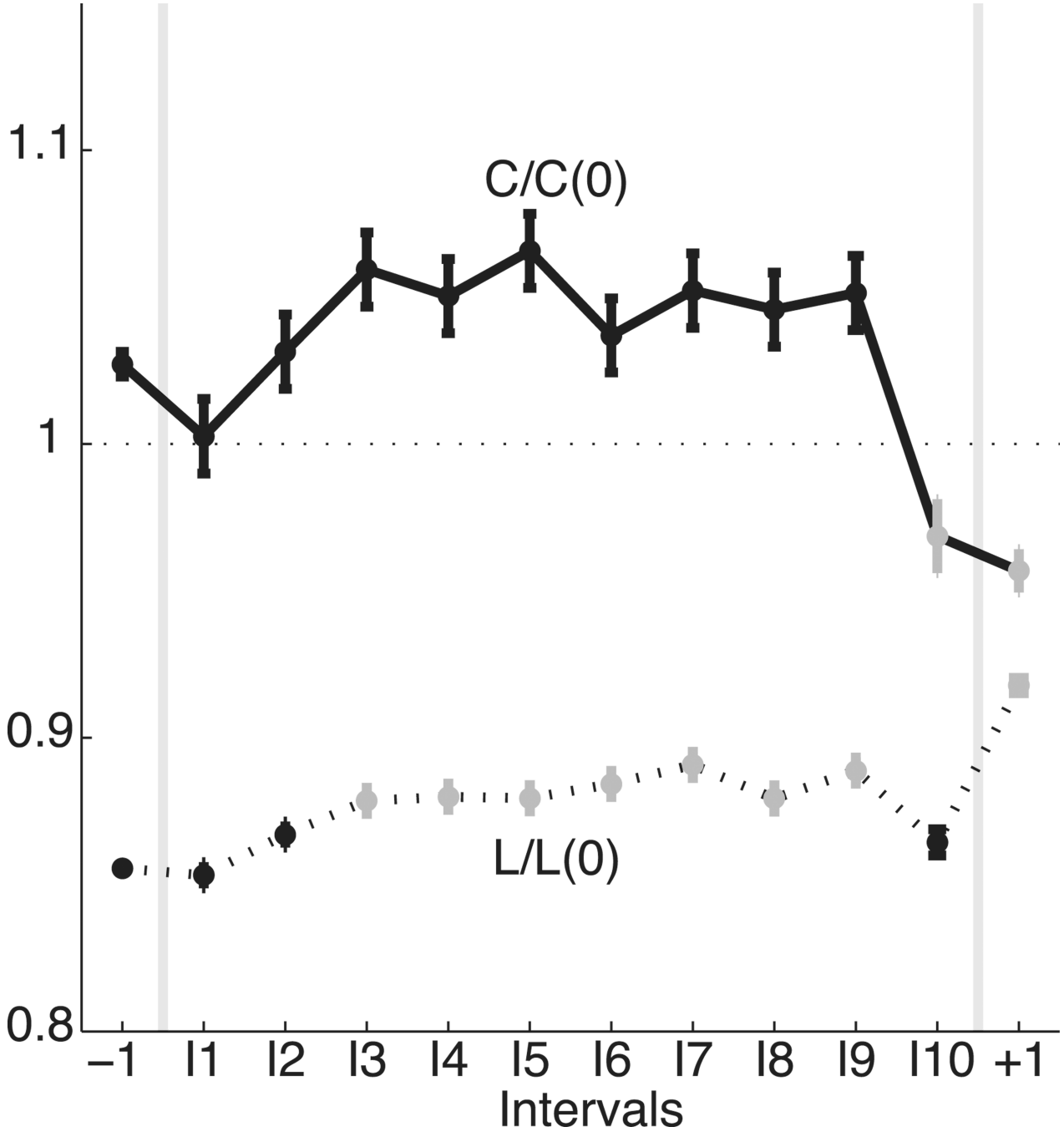

Figure 3.

The topological properties of the dominant subnetwork evolve during the seizure. We plot the scaled characteristic path length [L/L(0), dashed curve] and scaled clustering coefficient [C/C(0), solid curve] for each interval (adjusted for differences in subjects and with the same number of networks per interval as in Figure 1). Values that increase or decrease significantly from the preictal level are indicated in gray. For all intervals considered, the networks are approximately small-world. During the seizure, both measures tend to increase and the networks therefore become more regular. Just before seizure termination (interval I10), both measures decrease and the networks acquire a more random configuration.

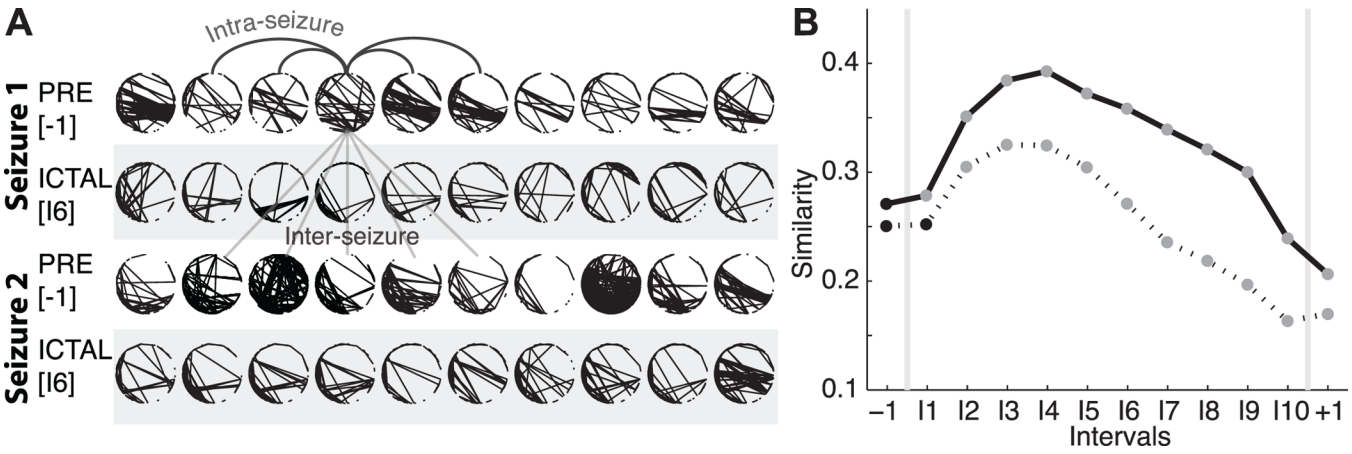

Figure 4.

Networks become more similar during — and between — seizures. **(A)** Two examples of networks from a preictal interval (unshaded) and ictal interval (shaded) from two different seizures of a single subject. Visual inspection suggests that the ictal networks are more similar both within each seizure (i.e., within each shaded region), and between the two seizures (i.e., between the two shaded regions), compared to the preictal networks. The arched (straight) lines indicate example intra-seizure (inter-seizure) comparisons. **(B)** The similarity between networks within each interval of the same seizure (i.e., intra-seizure similarity, solid curve) and between intervals of different seizures from the same subject (i.e., the inter-seizure similarity, dashed curve). The intra-seizure similarity increases during seizure; networks become more similar within ictal intervals compared to preictal intervals. The inter-seizure similarity, which compares networks from the same interval but different seizures of a subject, also increases during seizure. For both curves, circles denote the mean value (n={82059, 10222, 30666}) of intra-seizure comparisons for the preictal, ictal, and postictal intervals, respectively, and n={277537, 40169, and 120507} inter-seizure comparisons for the preictal, ictal, and postictal intervals, respectively, adjusted for differences in subjects; the vertical lines denoting the standard error are no larger than the black or gray circles. Statistically significant changes from the preictal value are indicated in gray (see Methods).

Table 1

Patient characteristics. Age at onset indicates the age at which seizures are first described by the patient. For each subject, *N* seizures were analyzed with durations listed in the fifth column. “Grids” and “strips” refer to surface (pial) electrode arrays which were also always accompanied by depth electrodes. “Depths” refer to patients who only received orthogonal placement of intraparenchymal arrays of electrodes. The total number of intracranial electrodes and the number of electrodes involved at seizure onset are listed for the dominant seizure type. All seizure types were either complex partial seizures which had secondary generalization (CPS+2nd), complex partial seizures without secondary generalization (CPS), or simple partial seizures (SPS); the number of each type of seizure for each patient is indicated. The frequency bands of maximum power at seizure onset were estimated using standard power spectrum analysis. Power spectra (Hann taper) were computed for 1s of ECoG data immediately following clinical determination of seizure initiation and averaged over the onset electrodes. Beta=15–30 Hz, Alpha=8–12 Hz, Theta=4–8 Hz, Delta=1–4 Hz. The etiology based on history, imaging and seizure semiology refers to a diagnosis made by the clinical team with all available data prior to implantation of electrodes, surgical resection and pathological examination of resected tissue. The etiology based on pathology comes directly from the clinical determination made by neuropathologists. The lobe of involvement was determined by examination of the seizure onsets on the intracranial recording electrodes. MTS = mesial temporal sclerosis. Etiology notes: 1) Bilateral onsets – no resection performed, 2) Eloquent cortex – no resection performed, 3) Patient decided not to go forward with resection.

Patient	Sex	Age at Onset / Surgery	*N*	Duration of seizures (s)	Electrodes	Electrodes total / onset	Seizure type (Number)	Onset activity	Etiology	Etiology (based on pathology)	Lobe of involvement
A	M	3 / 37	4	76, 63, 61,134	Grids, strips and depths	100 / 5	CPS+2nd (4)	Beta, Alpha, Delta	Unknown	No significant abnormalities	Temporal (lateral)
B	F	20 / 45	4	114, 102, 121, 142	Depths	65 / 5	CPS+2nd (4)	Delta	Temporal lobe - MTS	No pathology obtained [1]	Temporal (mesial)
C	F	15 / 46	5	87, 93, 102, 100, 112	Grids, strips and depths	122 / 5	CPS+2nd (5)	Beta, Alpha, Delta	Cortical Dysplasia	Cortical Dysplasia	Temporo-parieto-occipital
D	F	17 / 45	3	80, 82, 42	Depths	40 / 2	CPS+2nd, CPS (2,1)	Beta, Delta	Possible post-infectious	No pathology obtained [2]	Parieto-Occipital
E	M	7 / 22	2	87, 92	Grids, strips and depths	124 / 4	CPS+2nd (2)	Delta	Cortical Dysplasia	Cortical Dysplasia	Frontal (cingulate)
F	F	14 / 28	4	331, 111, 84, 128	Grids, strips and depths	94 / 22	CPS+2nd, CPS, SPS (1,1,2)	Delta	Encephalitis	Reactive gliosis	Temporal (mesial)
G	M	17 / 29	7	93, 137, 104, 134, 156, 179, 101	Depths	70 / 2	CPS, SPS (5,2)	Delta	Traumatic Brain Injury	Reactive gliosis	Temporal (mesial)
H	F	13 / 31	2	65, 90	Depths	34 / 4	CPS (2)	Delta	Temporal lobe - MTS	No significant abnormalities	Temporal (mesial)

Patient	Sex	Age at Onset / Surgery	*N*	Duration of seizures (s)	Electrodes	Electrodes total / onset	Seizure type (Number)	Onset activity	Etiology	Etiology (based on pathology)	Lobe of involvement
I	M	43 / 45	8	55, 57, 63, 49, 58, 199, 54, 90	Depths	64 / 4	CPS+2nd, CPS, SPS (1,1,6)	Alpha, Delta	Unknown	No pathology obtained [1]	Temporal (mesial and lateral)
J	M	14 / 19	4	82, 138, 123, 40	Grids, strips and depths	80 / 3	SPS (4)	Alpha, Delta	Temporal lobe - MTS	Hippocampal sclerosis	Temporo-parieto-occipital
K	F	59 / 65	5	171, 121, 105, 224, 133	Depths	68 / 2	CPS, SPS (4,1)	Beta, Alpha	Unknown	No pathology obtained [3]	Frontal (orbito-frontal)